

LOW ORDER ABERRATIONS IN BAND-LIMITED LYOT CORONAGRAPHS

ANAND SIVARAMAKRISHNAN¹, RÉMI SOUMMER^{1,2}
Space Telescope Science Institute
3700 San Martin Drive, Baltimore, MD 21218

ALLIC V. SIVARAMAKRISHNAN
Choate Rosemary Hall School
333 Christian Street, Wallingford, CT 06492

JAMES P. LLOYD¹
Astronomy Department
230 Space Sciences Building
Cornell University, Ithaca, NY 14853

BEN R. OPPENHEIMER
Astrophysics Department, American Museum of Natural History
Central Park West at 79th Street, New York, NY 10024

AND

RUSSELL B. MAKIDON¹
Space Telescope Science Institute
3700 San Martin Drive, Baltimore, MD 21218
ApJ, accepted

ABSTRACT

We study the way Lyot coronagraphs with unapodized entrance pupils respond to small, low order phase aberrations. This study is applicable to ground-based adaptive optics coronagraphs operating at 90% and higher Strehl ratios, as well as to some space-based coronagraphs with intrinsically higher Strehl ratio imaging. We utilize a second order expansion of the monochromatic point-spread function (written as a power spectrum of a power series in the phase aberration over clear aperture) to derive analytical expressions for the response of a ‘band-limited’ Lyot coronagraph (BLC) to small, low order, phase aberrations. The BLC possesses a focal plane mask with an occulting spot whose opacity profile is a spatially band-limited function rather than a hard-edged, opaque disk. The BLC is, to first order, insensitive to tilt and astigmatism. Undersizing the stop in the re-imaged pupil plane (the Lyot plane) following the focal plane mask can alleviate second order effects of astigmatism, at the expense of system throughput and angular resolution. The optimal degree of such undersizing depends on individual instrument designs and goals. Our analytical work engenders physical insight, and complements existing numerical work on this subject. Our methods can be extended to treat the passage of higher order aberrations through band-limited Lyot coronagraphs, by using our polynomial decomposition or an analogous Fourier approach.

Subject headings: instrumentation: adaptive optics — space vehicles: instruments — techniques: image processing — astrobology — circumstellar matter — planetary systems

1. INTRODUCTION

Lyot coronagraphy (Lyot 1930, 1939) has enjoyed a resurgence because interest in discovering and characterizing extrasolar planets has been stimulated by advances in ground-based adaptive optics (AO), as well as support from space agencies for extrasolar planetary science missions. There is currently one extreme adaptive optics (ExAO) coronagraph being used to conduct a complete complete survey for faint companions and disks around nearby stars (Oppenheimer et al. 2003, 2004; Digby et al. 2004; Makidon et al. 2005). New coronagraph designs to enable the detection

and characterization of extrasolar planets abound (Nisenson & Papaliolios 2001; Aime et al. 2002; Kuchner & Traub 2002; Soummer et al. 2003a,b; Aime & Soummer 2003; Kasdin et al. 2003; Soummer 2005). Many of these designs would suppress light from the central star around which a planet orbits, as long as the telescope and instrument optics and stops were perfect, and simple Fourier optics theory was accurate enough to predict instrument behavior in these high contrast regimes. Less-than-ideal image quality is a stumbling block which impedes attainment of this science goal. Kasdin (private communication) has demonstrated in the laboratory that Fourier optics appears to be valid down to contrast ratios of 10^{-7} .

We study the way Lyot coronagraphs dedicated to

¹ NSF Center for Adaptive Optics.

² Michelson Post-doctoral Fellow.

imaging extrasolar Jovian and terrestrial planets respond to small, low order phase aberrations. Perrin et al. (2003) demonstrated that for ground-based adaptive optics systems delivering Strehl ratios of at least 90%, a second-order expansion of the imaging system’s point-spread function (PSF) response to monochromatic light from a point source (Sivaramakrishnan et al. 2002) was sufficient to model the effects of phase aberrations on the PSF. We analyze the case of unapodized telescopes in high dynamic range regimes, as is relevant to the problem of tolerancing optics on space-based coronagraphic telescopes or calibrating wavefront sensing non-common path errors on ground-based ExAO instruments dedicated to finding and characterizing extrasolar planets.

Lloyd & Sivaramakrishnan (2005) derived the response of a simple band-limited coronagraph to small tilt errors, using an analytical method combined with an expansion of the pupil plane field strength (defined later) in terms of the phase aberration over the pupil. That work produced insight into the way tilt error causes light to leak through a coronagraph that is designed to suppress all light from a perfectly flat, on-axis wavefront. Such an analytical treatment develops a qualitative understanding of coronagraphic response to phase errors. Insights developed there apply to classical Lyot coronagraphy. We extend the methods of Lloyd & Sivaramakrishnan (2005) to understand how low order aberrations propagate through a band-limited Lyot coronagraph. While earlier studies (*e.g.*, Malbet 1996; Sivaramakrishnan et al. 2001; Green et al. 2003) explored some aspects of coronagraphy on imperfect wavefronts, they did not provide analytical tools required to understand some of the optical problems of designing a coronagraph to achieve the 10^7 photometric dynamic range needed by a space mission dedicated to discovering and characterizing extrasolar Jovian planets, or the 10^{10} contrast ratio that extrasolar terrestrial planet discovery may well demand (Breckinridge & Oppenheimer 2004). Our analytical approach is a start along the route to understanding coronagraphic data described in *e.g.*, Oppenheimer et al. (2004); Digby et al. (2004).

A band-limited coronagraph is a perfect coronagraph design in that simple Fourier optics modelling suggests that it will prevent all incoming, on-axis light from reaching the final coronagraphic focal plane. We define light leak as the fraction of incident on-axis energy that reaches the final coronagraphic focal plane. Our concern is restricted to diffractive light leak rather than light redistributed within the instrument by scattering off imperfect optics. We also concentrate on small aberrations of the wavefront that forms the first image. For instance, we treat tilts that are small compared to the angular resolution of the system. Such tilts decenter the star behind the focal plane mask’s occulting spot without moving it out from behind the spot — which is itself at least a few resolution elements in diameter. Such aberrations in the wavefront prior to the focal plane mask result in light leaking through a supposedly perfect coronagraph, reaching the final coronagraphic image plane, thereby reducing the dynamic range of the instrument. We find that small amounts of tilt and astigmatism do not increase the light leak through the coronagraph, whereas the same amounts of coma and spherical aberration do. However, detrimental second order effects of astigmatism

can be reduced by undersizing the Lyot stop. Our analysis shows that defocus and tilt produce characteristic intensity distributions in the Lyot plane, which suggests ways this signal can be used to align a high dynamic range coronagraph, and calibrate the offset between the focal plane mask location in the final coronagraphic image plane, thereby improving the coronagraph’s astrometric accuracy. Similar analyses on the various coronagraph designs being developed for the purpose of detecting Jovian and Earth-like planets around nearby stars will contribute to an informed selection of a design, in addition to providing insight into how to improve these designs.

2. BASIC CORONAGRAPHIC THEORY

A simple mathematical description of the fundamentals of Lyot coronagraphy (Lyot 1939) can be found in Sivaramakrishnan et al. (2001), Aime & Soummer (2002), Lloyd & Sivaramakrishnan (2005), and references therein.

2.1. Monochromatic coronagraphic theory

Here we briefly recapitulate our basic monochromatic Fourier optics formalism, which follows that of Lloyd & Sivaramakrishnan (2005); Sivaramakrishnan & Lloyd (2005). A more detailed treatment can be found in Born & Wolf (1993). We recollect that a plane monochromatic wave travelling in the z direction in a homogenous medium without loss of energy can be characterized by a complex amplitude E representing the transverse (*e.g.*, electric) field strength of the wave. The full spatio-temporal expression for the field strength is $Ee^{i(\kappa z - \omega t)}$, where $\omega/\kappa = c$, the speed of the wave. We do not use the term *field* to denote image planes — the traditional optics usage — we always use the term to denote electromagnetic fields or scalar simplifications of them. The wavelength of the wave is $\lambda = 2\pi/\kappa$. The time-averaged intensity of a wave at a point is proportional to EE^* , where the average is taken over one period, $T = 2\pi/\omega$, of the harmonic wave. The phase of the complex number E represents a phase difference from the reference phase associated with the wave. A real, positive E corresponds to an electric field oscillating in phase with our reference wave. A purely imaginary positive value of E indicates that the electric field lags by a quarter cycle from the reference travelling wave. Transmission through passive, linear filters such as apertures, apodizers, and so forth, is represented by multiplying the field strength by the transmission of these objects which modify the wave. Again, such multiplicative modification is accomplished using complex numbers to represent phase changes forced on the wave incident on such objects.

We assume that scalar Fourier optics describes our imaging system (cf. Breckinridge & Oppenheimer 2004): image field strengths are given by the Fourier transform of aperture (or pupil — we use the two terms interchangeably) illumination functions, and vice versa.

A telescope aperture is described by a transmission function pattern $A(\mathbf{x})$, where $\mathbf{x} = (x, y)$ is the location in the aperture, in units of the wavelength of the light (see Fig. 1). The corresponding aperture illumination describing the electric field strength in the pupil (in response to an unaberrated, unit field strength, monochro-

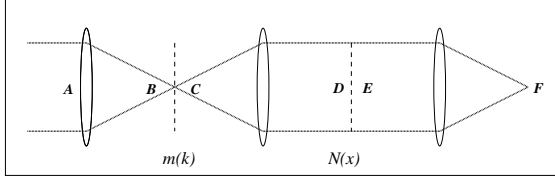


FIG. 1.— The essential planes and stops in a coronagraph. The entrance aperture is A, the direct image at B falls on a focal plane mask whose transmission function is $m(k)$. The re-imaged pupil plane D, after being modified by passage through a Lyot stop with a transmission function $N(x)$, is sent to the coronagraphic image at F. A, D, and E are pupil planes, and B, C, and F are image planes.

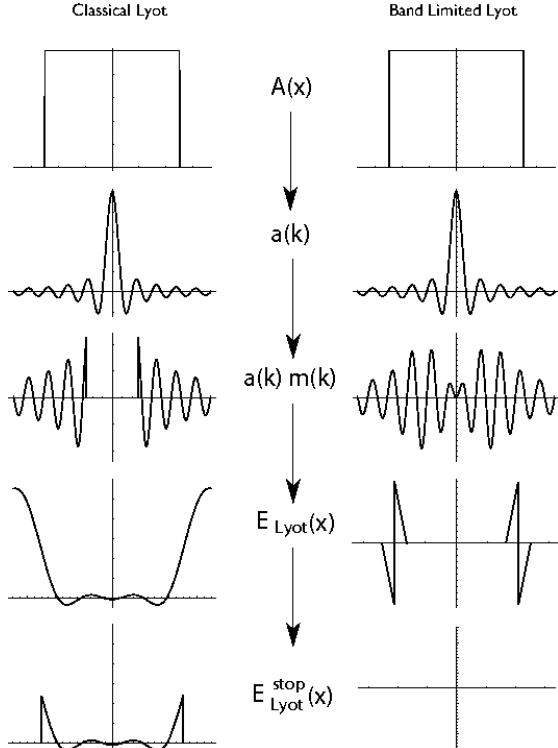


FIG. 2.— A sketch of the classical Lyot coronagraph (left), and the 1 - sinc “top-hat” band-limited coronagraph operating on a perfectly flat incoming wavefront. The top row shows the same aperture function used in both examples, *viz.*, a clear unobscured entrance aperture. The second row shows the field strength at the image plane. The third row shows the field strength immediately after passage through the focal plane mask. The classical Lyot, on the left, has a hard-edged, opaque mask. This band-limited coronagraph has a mask that is opaque only at its center. The fourth row shows the field strength in the Lyot pupil plane before a Lyot stop is applied, and the final row shows the field after the Lyot stop in the Lyot pupil plane. The band-limited coronagraph blocks all incoming on-axis light if the wavefront is unaberrated.

matic incident wave) is $E_A = A(\mathbf{x})$. From this point onwards we drop the common factor $Ee^{(i\kappa z - \omega t)}$ when describing fields. The aperture intensities ($E_A E_A^*$) for two coronagraphic designs are shown in Fig. 2 (top row). The field strength in the image plane, $E_B = a(\mathbf{k})$, is the Fourier transform of E_A , where $\mathbf{k} = (k_x, k_y)$ is the image plane coordinate in radians. Because of the Fourier relationship between pupil and image fields, \mathbf{k} is also a spatial frequency vector for a given wavelength of light. We refer to this complex-valued field a as the ‘amplitude-spread function’ (ASF), by analogy with the PSF of an optical

system. The PSF is aa^* . Our convention is to change the case of a function to indicate its Fourier transform. We multiply the image field E_B by a mask function $m(\mathbf{k})$ to model the focal plane mask of a coronagraph. The image field immediately after this mask is $E_C = m(\mathbf{k}) E_B$. The electric field in the re-imaged pupil after the focal plane mask is E_D , which is the Fourier transform of E_C . We use the fact that the transform of the image plane field E_B is just the aperture illumination function E_A itself, so the Lyot pupil field is $E_D = M(\mathbf{x}) * E_A$, where $*$ is the convolution operator.

If the Lyot pupil stop transmission is $N(\mathbf{x})$, the electric field after the Lyot stop is $E_E = N(\mathbf{x}) E_D$. The transform of this last expression is the final coronagraphic image field strength: $E_F = n(\mathbf{k}) * [m(\mathbf{k}) E_B]$.

The aperture illumination function with phase aberrations is

$$A_{aber} = A(\mathbf{x}) e^{i\phi(\mathbf{x})}. \quad (1)$$

In this paper we look at the way small phase aberrations $\phi(\mathbf{x})$ pass through a band-limited coronagraph. Our approach is to expand the exponential in equation (1) in powers of $\phi(\mathbf{x})$, so the quantity that determines the rate of convergence of the expansion is the largest excursion of ϕ from its mean value over the clear aperture.

2.2. The Lyot plane field

A coronagraphic stop is modelled by multiplying the image field by a focal plane mask transmission function $m(\mathbf{k})$, so the electric field strength just after the focal plane mask is $a_{aber} m$. When describing a Lyot coronagraph it is sometimes helpful to introduce a ‘mask shape function’ w by the definition

$$m(\mathbf{k}) \equiv 1 - w(\mathbf{k}). \quad (2)$$

When w is unity at the origin the mask is opaque at its center. We can write the electric field at the Lyot plane as

$$E_{Lyot}(\mathbf{x}) = A_{aber} * (\delta(\mathbf{x}) - W(\mathbf{x})) = A_{aber} - A_{aber} * W(\mathbf{x}). \quad (3)$$

Understanding the subtleties of this equation in the case of high Strehl ratio imaging is essential to understanding how small phase aberrations cause light to leak through a coronagraph designed to produce perfect on-axis image suppression with completely unaberrated on-axis light.

2.3. Band-limited coronagraphs

Kuchner & Traub (2002) use a focal plane mask shape function w which is band-limited. This means that there is a minimum positive value of b such that the mask function’s FT, W , satisfies the property

$$W(\mathbf{x}) = 0 \text{ if } |\mathbf{x}| > b. \quad (4)$$

The bandwidth or bandpass of w is b (note that b is actually a physical distance in pupil space). We select the mask function in its transform (pupil) space, (x, y) , rather than in physical (image) space, (k_x, k_y) , even though it is applied in the image plane in any real coronagraph. If the telescope diameter is D , then the characteristic scale of the mask function is D/b resolution elements (a resolution element is λ/D radians, λ being the wavelength of the monochromatic light). This results in a focal plane mask about D/b Airy rings in size.

2.4. The top-hat band-limited coronagraph

The simplest choice for $W(\mathbf{x})$ is the ‘top-hat’ function $\Pi(x/d, y/d)/d^2$, where

$$\begin{aligned} \Pi(x, y) &= 1 \text{ for } |x| < 1/2, |y| < 1/2, \\ \Pi(x, y) &= 0 \text{ elsewhere} \end{aligned} \quad (5)$$

(see Fig. 2). The bandwidth of the corresponding mask function is $d/2$. A normalizing factor of $1/d^2$ is applied to ensure that the area under $W(\mathbf{x})$ is unity, thus ensuring that $w(0,0) = 1$; the focal plane mask is opaque at its center. A top-hat W produces a multiplicative image stop function

$$m(\mathbf{k}) = 1 - \text{sinc}(dk_x) \text{sinc}(dk_y). \quad (6)$$

Our interest such a choice is primarily didactic: this coronagraph leaks aberrated light in a manner similar to that of the more popular ‘sawtooth’ band-limited coronagraph, *viz.*, one with a mask function FT of

$$W(x, y) = \Lambda(x/d, y/d)/d^2 = \Lambda(x/d)\Lambda(y/d)/d^2, \quad (7)$$

where

$$\begin{aligned} \Lambda(x) &= |1 - x| \text{ for } |x| < 1, \\ \Lambda(x) &= 0 \text{ elsewhere.} \end{aligned} \quad (8)$$

The sawtooth coronagraph has a focal plane mask described by $m(\mathbf{k}) = 1 - \text{sinc}^2(dk_x) \text{sinc}^2(dk_y)$.

3. EXPANSION USING THE PHASE FUNCTION

The phasor $e^{i\phi}$ can be expanded as $1 + i\phi - \phi^2/2! + \dots$ for any finite value of the aberration ϕ . Depending on the size of the aberration it is useful to truncate this expansion at various orders (*e.g.*, Bloemhof et al. 2001; Sivaramakrishnan et al. 2002; Perrin et al. 2003). The first order perturbation of the field strength in the aperture is imaginary: *i.e.*, the field due to phase aberrations is in phase-quadrature to the perfect aperture field. The second order aberration of the aperture field strength is in (anti-)phase with the perfect wave’s field strength.

3.1. Zernike polynomials and Cartesian expansions

Zernike polynomials, which are a set of orthogonal polynomials on the unit radius 2-dimensional disk, are frequently used to describe phase aberrations in optical systems (*e.g.*, Born & Wolf 1993; Noll 1976). These polynomials are expressible in either circular coordinates (r, θ) or Cartesian coordinates (x, y) . Expressing Zernike polynomials in Cartesian coordinates leads to a mathematical simplicity that promotes a better understanding of the physics of an imperfect band-limited Lyot coronagraph. Because of this, we investigate coronagraphy on a square aperture in order to make integrals separable in x and y .

We have the choice of writing the phase as either a simple polynomial or an expansion in terms of Zernikes. In the latter case, we must choose the Zernike functions’ normalized coordinates: we choose the disk on which we define our Zernike functions to possess an area equal to that of our square aperture. This choice results in extrapolating the Zernike polynomials to a radial coordinate of $2/\sqrt{\pi} \simeq 1.128$, which is beyond their usual range of validity. Doing so is a fruitful exercise if we restrict ourselves to low order aberrations. We emphasize that we do not invoke any of the Zernike polynomials’ orthonormal properties to prove any result. Thus our apparently

cavalier extrapolation of the polynomials beyond the domain over which they are usually defined does not lead to grief. We only use them here because they are widely used in the optical literature. A more natural Fourier decomposition of the phase aberration over the aperture is of course possible, and may even be preferable to a Zernike decomposition for higher order aberrations.

Our choice of the equal-area circle for our Zernike polynomials is motivated by the following considerations: if we use the circumscribing circle around our square aperture, we miss the steep increases of Zernike functions describing *e.g.*, spherical aberration at the edge of the disk, which for the most part will lie outside our square aperture. If we use an inscribed circle, we include large areas in the corners of the apertures where the magnitude of the third, fourth, and fifth order polynomials increase sharply, contributing features that we do not commonly associate with particular Zernike aberrations. Instead of either extreme, we stick to the middle ground, at the expense of mathematical purity: we miss some of the higher values of these Zernike polynomials where our circle extends outside the square aperture, but collect larger phase errors at the corners of our aperture, where the normalized Zernike arguments exceed unity. The net effect of this is that we can still talk about Zernike functions on our square aperture, in much the same way Zernike function aberrations on obscured apertures such as HST or Palomar are discussed, even though the annular Zernike functions of Mahajan (1981) should be used on annular apertures.

4. PROPAGATION OF SIMPLE POLYNOMIAL PHASE ABERRATIONS

At any location in the pupil plane, A_{aber} can be expanded in an absolutely convergent series in ϕ for any finite value of the phase function:

$$A_{aber} = AA_\phi = A(1 + i\phi - \phi^2/2 + \dots). \quad (9)$$

If the phase over the aperture is expressed by

$$\begin{aligned} \phi(x, y) &= \sum_{i=1}^{\infty} a_i Z_i(x, y) \\ &= \sum_{n=0, m=0}^{\infty} \alpha_{mn} x^n y^m, \end{aligned} \quad (10)$$

where the Z_i ’s are Zernike polynomials, and a_i, α_{mn} are constant coefficients, then equation (9) produces first, second, and higher order terms in x and y . A measure of the magnitude of the phase aberration — ϵ , the largest absolute value of the deviation of the phase ϕ from its aperture-weighted mean — can be used to estimate the size of a particular order term in equation (9). Given any particular value of ϵ one can estimate where the terms in the above expansion become negligible (Perrin et al. 2003). For example, in the Advanced Camera for Surveys (ACS) coronagraph on the Hubble Space Telescope (HST), which sits in the aberrated beam, with about half a wave of spherical aberration at a wavelength of 800nm, one must use about seven terms of the above expansion to model the gross features of the aberrated field strength over the aperture.

4.1. Power leak through a top-hat band-limited coronagraph

We can calculate how an arbitrary polynomial phase aberration of the form $\alpha_{nm}x^n y^m$ propagates through the coronagraph to the Lyot plane, using this expansion. The calculation is straightforward for a square aperture because the limits of integration and the basis functions are separable. From equation (3) we see that the Lyot field for such an aberration is described by

$$E_{Lyot}(x, y) = A(x, y)\alpha_{nm}x^n y^m - \Pi(x/d, y/d)/d^2 * [A(x, y)\alpha_{nm}x^n y^m] \quad (11)$$

for the ‘top-hat’ band-limited coronagraph design. This calculation becomes difficult to perform analytically when the mask transform function has a more extended support, as in a classical Lyot design.

We define the function

$$L_{\Pi,n}(x, d) = \Pi(x/d) * x^n / d, \quad (12)$$

which enables us to write equation (11) as

$$E_{Lyot}(x, y) = \alpha_{nm}x^n y^m - \alpha_{nm}L_{\Pi,n}(x, d)L_{\Pi,m}(y, d) \quad (13)$$

in the interior of the Lyot plane in the case of unapodized apertures. We define the interior of the aperture as that part of the aperture (or image of the aperture, such as the Lyot plane) which is further than b from any point on the aperture boundary (where b is the bandwidth of the mask shape function). This is the area of the Lyot pupil which would not be obstructed by a Lyot stop in a perfect band-limited coronagraph (see Kuchner & Traub 2002; Lloyd & Sivaramakrishnan 2005; Sivaramakrishnan & Lloyd 2005, for further detail). The aperture function $A(\mathbf{x})$ is unity everywhere in the interior of the aperture for an unapodized entrance pupil, and so does not appear explicitly in equation (13).

The 2.4 m HST ACS coronagraph has an image plane stop diameter of $1''/8$, or ~ 30 resolution elements at 800 nm. Therefore the results we derive here for band-limited coronagraphs apply even though the ACS coronagraph is not band-limited, because its Lyot plane can be said to possess an ‘interior’ area which is further than a few $D/30$ scale lengths away from the annular aperture boundaries (see Sivaramakrishnan et al. 2001, for a discussion of the natural scale length in the Lyot plane).

Explicit evaluation $L_{\Pi,n}(x, d)$ is a matter of straightforward integration: the first few values of n produce

$$\begin{aligned} 1 - L_{\Pi,0}(x, d) &= 0 \\ x - L_{\Pi,1}(x, d) &= 0 \\ x^2 - L_{\Pi,2}(x, d) &= -d^2/12 \\ x^3 - L_{\Pi,3}(x, d) &= -d^2x/4 \\ x^4 - L_{\Pi,4}(x, d) &= -d^2x^2/2 - d^4/80 \\ x^5 - L_{\Pi,5}(x, d) &= -5d^2x^3/6 - d^4x/16 \\ x^6 - L_{\Pi,6}(x, d) &= -5d^2x^4/4 - 3d^4x^2/16 - d^6/448. \end{aligned} \quad (14)$$

The right hand sides of these equations are the first order residual Lyot field strength given a small phase aberration of $\alpha_n x^n$ over the entrance pupil of a one-dimensional band-limited coronagraph.

Low order phase aberrations, along with the resultant first and second order Lyot plane intensities are shown

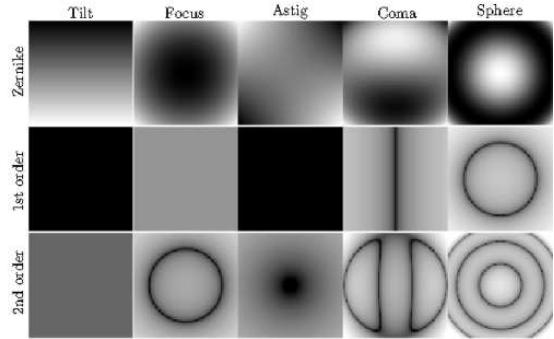


FIG. 3.— Response of the 1 – sinc ‘top-hat’ band-limited coronagraph to tilt, astigmatism, focus, coma and spherical aberrations. Each aberration shown produces a 95% Strehl ratio direct image. Phase aberrations (top row) result in non-zero intensity in the Lyot pupil interior. Analytical first order (middle row) and second order (bottom row) approximations to these intensities are shown on a logarithmic grey scale, between 0.1 (white) and 10^{-7} (black). First order power leak through the BLC due to tilt and astigmatism are identically zero. Defocus, and second order tilt cause uniform illumination in the Lyot pupil interior, which produces a fainter version of the direct PSF (although with a larger resolution element due to Lyot stop undersizing) in the final coronagraphic image.

in each column of Fig. 3. The band limit of this coronagraph is $b = D/5$. The fraction of incident power leaking through into the Lyot plane interior is presented in Table 1. Each power leak fraction is renormalized by dividing by the fractional coronagraphic throughput, which is the ratio of the areas of the optimal Lyot stop and the entrance aperture. For a band limit of $D/5$ this ratio is $9/25$ (e.g., Sivaramakrishnan et al. 2001).

5. EXTENSION TO THE SAWTOOTH BAND-LIMITED CORONAGRAPH

Designs similar to the sawtooth (sinc-squared focal plane mask function) coronagraph are being considered for the James Webb Space Telescope’s Near Infrared Camera, as well as for a dedicated coronagraphic space telescope. In order to calculate how the sawtooth band-limited coronagraph leaks low order aberrations, we can define a function $L_{\Lambda,0}(x, d)$ using the analogy of equation (12):

$$L_{\Lambda,n}(x, d) = \Lambda(x/d) * x^n / d, \quad (15)$$

and carry out the same analysis as in section 4.1. We present the top-hat band-limited coronagraph’s response to low order aberrations (Fig. 3); the sawtooth coronagraph’s response is qualitatively similar. The latter coronagraph’s mask function’s Fourier transform is a sawtooth function, which also yields tractable algebraic expressions for the Lyot pupil field strength for any order. For the sawtooth design the residual Lyot field in the interior of the Lyot plane has similar algebraic properties to that of the top-hat design. The powers of the relevant physical quantities for the $1 - \text{sinc}^2$ mask function of the sawtooth coronagraph are the same as those in equation (14), although the numerical coefficients differ slightly.

6. SECONDARY MIRROR ALIGNMENT ERRORS

When considering a simple on-axis two-mirror telescope, errors in positioning the secondary mirror result in aberrations described by a few low order Zernike polynomials.

Off-axis designs may have different sensitivities, but their phase aberrations due to secondary mirror tilt, despace, and decenter are still described by combinations of low order polynomials.

6.1. Sensitivity to stop size

The amount of energy leaking into the interior of the Lyot pupil is proportional to the fourth power of the bandwidth of the stop, or the inverse fourth power of the stop size expressed in resolution elements. This follows from inspection of equation (14). The leaked energy finds its way into the final image plane, unless the Lyot stop is adjusted to block some of this light. This strong dependence must play a significant role when choosing a coronagraph design given a desired contrast ratio derived from a scientific goal.

6.2. Crosstalk between aberrations

When two aberration, either simple monomials or Zernike polynomials, are present simultaneously, the Lyot pupil field contains energy due to a ‘crosstalk’ term in addition to effects from each individual term, even in the first order calculation. Cataloguing the various crosstalk energy leaks is beyond the scope of this work: we restrict ourselves to a few simple, traditional aberrations.

6.3. The effects of tilt and defocus

Equation (14) demonstrates that for a band-limited coronagraph there is complete cancellation of the central source even for small tilt errors ($L_{\Pi,1} = 0$). This particular result has already been derived by Kuchner & Traub (2002); Lloyd & Sivaramakrishnan (2005): here it is derived as part of the band-limited coronagraph’s response to a sequence of small polynomial phase errors.

The way focus affects the field strength in the interior of the Lyot plane can be found by inspection of the $L_{\Pi,2}$ term in equation (14). Given an aberration of the form $\alpha(x^2 + y^2)$, the field strength in the interior of the Lyot plane is $\alpha d^2/6$, to first order. The interior of our coronagraph’s Lyot plane fills uniformly with in-phase light. The effective telescope diameter describing the residual PSF for a circular aperture is $D - 2d$, so a fraction $\alpha^2 d^4 (1 - 2d/D)^2 / 36$ of incident power leaks through the coronagraph. It is distributed in an Airy pattern corresponding to an aperture $D - 2d$ in diameter, assuming an optimally undersized Lyot stop is used.

In the absence of other aberrations, this places a ‘ghostly PSF’ with a calculable intensity in the final image. The form of this PSF for a circular unobstructed entrance aperture is just the Airy pattern of the undersized Lyot stop used in the coronagraph. This residual PSF is not to be confused with the spot of Arago (Born & Wolf 1993), whose intensity varies with occulter size, depending on the relative size of an occulter in the pupil plane and the Fresnel zones it obscures. The spot of Arago’s brightness fluctuates in intensity as one increases the pupil plane occulter size. The leaked PSF power we describe here does not possess undulating fluctuations, characteristic of the spot of Arago. The spot of Arago occurs with unaberrated wavefronts, whereas this leaked PSF is entirely dependent on the presence of aberrations in the wavefront.

The analytical result presented here leaves no unresolved questions pertaining to the numerical accuracy or rounding error. The approximations used in deriving this result become more accurate as the magnitude of the phase aberrations decrease, so this result is pertinent to coronagraphs designed for very high Strehl ratio, high dynamic range applications. The bandwidth of the focal plane mask function is the only coronagraphic parameter that enters into the light leak through the coronagraph due to inexact focus in these regimes.

We note in passing that if there is sufficient tilt error to merit a second order expansion of the pupil field strength, this second order tilt term will have a mathematically identical behavior to a small pure focus: a similar ‘ghostly’ PSF will appear in the final coronagraphic image. The fraction of incident power that leaks through the coronagraph can be calculated in a similar fashion to the way we estimate the power leak due to the first order effects of defocus. However, given the real or imaginary nature of the coefficients in the expansion of the electric field in terms of the phase, the second order effect of tilt is in quadrature with the first order focus term (the former being purely imaginary, the latter real), so the two cannot be made to cancel each other: they will add power to the Lyot field (and the final coronagraphic PSF) in quadrature.

If there is sufficient defocus to warrant a second order expansion of the pupil field, the amount of light leaking through the interior of the Lyot stop increases dramatically (Fig. 3, second row, second column).

6.4. Astigmatism

Small amounts of astigmatism have no first order effect on the band-limited coronagraph. This is easy to understand because of the separability of the xy polynomial, and the nature of the convolution in the definition of equation (14). The second order astigmatic power leak into the Lyot plane is comparable to that of the second order tilt term, especially at the edges of the interior of the Lyot stop (Fig. 3, third column). Thus, off-axis telescope designs with residual astigmatism could be used with Lyot stops which are undersized relative to a Lyot stop tailored for perfect optics.

6.5. Coma and spherical aberration

Leak through an unapodized Lyot coronagraph is dependent on local curvature of the wavefront, so the first order leak due to these terms is high, especially at the edges of the Lyot pupil interior. First order light leak into the Lyot pupil interior due to spherical aberration has the same form as that of the second order leak due to defocus (Fig. 3), but, because of the relative quadrature of the first and second order field strengths, these aberrations cannot be used to cancel each other by design.

7. CONCLUSION

Analytical studies of the mathematically simple band-limited coronagraph provide us with tools to help evaluate coronagraphic behavior without the need for extensive numerical investigations. The analysis also helps identify design strategies to reduce coronagraphic sensitivity to selected aberrations. Our results suggest that off-axis unobscured high dynamic range apertures can

be allowed more astigmatism if the Lyot pupil of a band-limited coronagraph is reduced in size, thereby reducing the demands made upon the structural stability of the telescope.

The theory developed here suggests that the coronagraphic PSF of the nominally on-axis source can be used to determine best focus, by minimizing the on-axis intensity behind the focal plane mask, utilizing focus sweep data. If the imaging quality is sufficiently high, leaked power due to small tilts (*i.e.*, small decentration of the target behind the focal plane mask, rather than moving the target out from behind the spot) can be used to determine the location of the focal plane mask. This latter exercise would aid astrometric calibration of the coronagraph.

Further theoretical analyses of coronagraphic response to aberrations could assist coronagraph design and operational plans to be made, to improve the scientific productivity of high dynamic range space-based coronagraphs dedicated to detecting and characterizing extrasolar planets.

The authors wish to thank the Space Telescope Sci-

ence Institute's Research Programs Office and its Director's Discretionary Research Fund. We are grateful to P. E. Hodge, J. C. Hsu, P. Greenfield, J. T. Miller and N. Dencheva for their role in developing and supporting the Python Numarray module (Greenfield et al. 2002; Greenfield et al. 2003), wrapping the numerical Fourier transform library FFTW (Frigo & Johnson 1997) for Numarray, and providing support for matplotlib (Hunter 2005). R.S. is supported by NASA Michelson Postdoctoral Fellowship under contract to the Jet Propulsion Laboratory (JPL) funded by NASA. The JPL is managed for NASA by the California Institute of Technology, A.V.S. acknowledges support from Choate Rosemary Hall School, and J.P.L. was supported in part by the California Institute of Technology's Millikan fellowship. This work is based upon work supported by the National Science Foundation under Grants No. AST-0215793, AST-0334916 and has also been supported by the National Science Foundation Science and Technology Center for Adaptive Optics, managed by the University of California at Santa Cruz under cooperative agreement No. AST-9876783.

REFERENCES

- Aime, C. & Soummer, R. 2002, in *Astronomy With High Contrast Imaging: from planetary systems to active galactic nuclei*, C. Aime & R. Soummer Eds (EAS Publication Series)
- Aime, C. & Soummer, R. 2003, *EAS Publications Series*, Volume 8, 2003. *Astronomy with High Contrast Imaging*, Proceedings of the conference held 13–16 May, 2002 in Nice, France. Edited by C. Aime and R. Soummer, 8
- Aime, C., Soummer, R., & Ferrari, A. 2002, *A&A*, 389, 334
- Bloemhof, E. E., Dekany, R. G., Troy, M., & Oppenheimer, B. R. 2001, *ApJ*, 558, L71
- Born, M. & Wolf, E. 1993, *Principles of Optics*, 6th ed. (Cambridge: Cambridge University Press)
- Breckinridge, J. B. & Oppenheimer, B. R. 2004, *ApJ*, 600, 1091
- Digby, A. P., Oppenheimer, B. R., Newburgh, L., Brenner, D., Shara, M., Mey, J., Mandeville, C., Makidon, R. B., Sivaramakrishnan, A., Soummer, R., Graham, J. R., Kalas, P., Perrin, M. D., Roberts, L. C., Kuhn, J., Whitman, K., & Lloyd, J. P. 2004, in *Proc. SPIE Vol. 5490, Advances in Adaptive Optics*, Roberto Ragazzoni and Domenico Bonaccini; Eds.
- Frigo, M. & Johnson, S. G. 1997, in *Technical Report MIT-LCS-TR-728* (Massachusetts Institute of Technology)
- Green, J. J., Shaklan, S. A., & Redding, D. C. 2003, in *Proc. SPIE, Vol. 4860, High-Contrast Imaging for Exo-planet Detection*, ed. A. B. Schultz & R. G. Lyon
- Greenfield, P., Miller, J. T., Hsu, J.-C., & White, R. L. 2003, in *PyCon 2003 Proceedings*, ed. S. Holden
- Greenfield, P., Miller, T., Hsu, J.-C., & White, R. L. 2002, in *ASP Conf. Ser. 281: Astronomical Data Analysis Software and Systems XI*, 140–+
- Hunter, J. 2005, *The Matplotlib User's Guide* (University of Chicago Medical School)
- Kasdin, N. J., Vanderbei, R. J., Spergel, D. N., & Littman, M. G. 2003, *ApJ*, 582, 1147
- Kuchner, M. J. & Traub, W. A. 2002, *ApJ*, 570, 900
- Lloyd, J. P. & Sivaramakrishnan, A. 2005, *ApJ*, 621, 1153
- Lyot, B. 1930, *C. R. Acad. Sci Paris*, 191, 834
- . 1939, *MNRAS*, 99, 580
- Mahajan, V. N. 1981, *JOSA*, 71, 75
- Makidon, R. B., Sivaramakrishnan, A., Perrin, M. D., Roberts, L. C., Oppenheimer, B. R., Soummer, R., & Graham, J. R. 2005, *PASP*, in press
- Malbet, F. 1996, *A&AS*, 115, 161
- Nisenson, P. & Papaliolios, C. 2001, *ApJL*, 549
- Noll, R. J. 1976, *Optical Society of America Journal*, 66, 207
- Oppenheimer, B. R., Digby, A. P., Newburgh, L., Brenner, D., Shara, M., Mey, J., Mandeville, C., Makidon, R. B., Sivaramakrishnan, A., Soummer, R., Graham, J. R., Kalas, P., Perrin, M. D., Roberts, L. C., Kuhn, J., Whitman, K., & Lloyd, J. P. 2004, in *Proc. SPIE Vol. 5490, Advances in Adaptive Optics*, Roberto Ragazzoni and Domenico Bonaccini; Eds.
- Oppenheimer, B. R., Sivaramakrishnan, A., & Makidon, R. B. 2003, *Imaging Exoplanets: The Role of Small Telescopes (The Future of Small Telescopes In The New Millennium. Volume III - Science in the Shadow of Giants)*, 155
- Perrin, M. D., Sivaramakrishnan, A., Makidon, R. B., Oppenheimer, B. R., & Graham, J. R. 2003, *ApJ*, 596, 702
- Sivaramakrishnan, A., Koresko, C. D., Makidon, R. B., Berkefeld, T., & Kuchner, M. J. 2001, *ApJ*, 552, 397
- Sivaramakrishnan, A. & Lloyd, J. P. 2005, *ApJ*, in press
- Sivaramakrishnan, A., Lloyd, J. P., Hodge, P. E., & Macintosh, B. A. 2002, *ApJ*, 581, L59
- Soummer, R. 2005, *ApJ*, 618, L161
- Soummer, R., Aime, C., & Falloon, P. 2003a, *A&A*, 397, 1161
- Soummer, R., Dohlen, K., & Aime, C. 2003b, *A&A*, 403, 369

TABLE 1
FIRST AND SECOND ORDER LEAK VS. STREHL RATIO

	99% Strehl		98% Strehl		95% Strehl	
	1 st Order Power	2 nd Order Power	1 st Order Power	2 nd Order Power	1 st Order Power	2 nd Order Power
Tilt	0	5.8×10^{-8}	0	2.3×10^{-7}	0	1.5×10^{-6}
Focus	1.8×10^{-5}	4.9×10^{-8}	3.6×10^{-5}	2.0×10^{-7}	9.1×10^{-5}	1.3×10^{-6}
Astig	0	2.3×10^{-9}	0	9.4×10^{-9}	0	6.1×10^{-8}
Coma	6.7×10^{-6}	5.0×10^{-9}	1.4×10^{-5}	2.0×10^{-8}	3.4×10^{-5}	1.3×10^{-7}
Sphere	5.8×10^{-5}	3.0×10^{-7}	1.2×10^{-4}	1.2×10^{-6}	3.0×10^{-4}	7.7×10^{-6}